Interpretation of Head-Gasket Ionization-Probe Measurements Using a Two-Zone Spherical Flame Model

P.O.Witze

Combustion Research Facility
Sandia National Laboratories
Livermore, CA 94551-0969
USA

ABSTRACT

An analytic procedure is described that uses the measured pressure and three-dimensional shape of the combustion chamber to rapidly calculate the time of contact of the ideal spherical flame with the known location of ionization probes in the walls of the combustion chamber. Differences between the measured and calculated flame arrival times are attributable to fluid mechanics and, to a lesser extent, mixture inhomogeneities. In either case, the ideal spherical flame serves as a reference point for improved understanding of the actual flame arrival measurements.

INTRODUCTION

The study of premixed-charge combustion in spark-ignition engines has a long history involving the use of multipoint measurements to determine the evolution of the burned gas volume in real time. In 1934, Schnauffer (1) installed twenty-four ionization probes throughout the head of an aviation engine. Because the electronics necessary to simultaneously record this many analog signals did not exist at the time, the ionization probes were wired to individual neon lamps arranged in a board at locations corresponding to the probe locations in the engine. As the propagating flame reached each probe, the lamps would light to reveal the evolution of the flame shape. The time of the lighting of the lamps could be determined on an individual basis using a stroboscope, or simultaneously by taking a high speed motion picture of the array of lamps.

Several decades later, Curry (2) installed forty-nine ionization probes in an engine head, and was able to record twenty-eight signals simultaneously on magnetic tape. The flame arrival time measurements obtained from these data were used to estimate the evolution of the burned gas volume. More recently, Spicher and coworkers (3,4) have installed as many as 240 small windows in an engine head, cylinder liner and piston. They used optical fibers to transmit the visible emissions collected through the windows to individual photodetectors, enabling measurements of flame position versus time. In all of these studies, because multiple point measurements were made along the path of flame surface propagation, it was possible to reconstruct the evolution of the burned gas volume with both spatial and temporal resolution. The disadvantage of the techniques is that considerable time and expense is required to install many probes throughout the combustion chamber.

In an effort to devise a more practical technique, Witze and coworkers (5,6) have shown that multiple ionization probes installed around the bore cutout in the head gasket can be used to measure the uniformity and cyclic variation of the arrival of the flame front at the perimeter of the cylinder. They typically use eight probes uniformly distributed around the bore, and present the results in a polar diagram format as shown in Fig. 1; these particular measurements were made in a production V-6 engine operated under two load conditions. Note that the radial rays in the polar diagram are not uniformly spaced. This is a result of drawing the rays with the origin at the spark gap, rather than at the cylinder axis. The direction of the rays is specified to pass through the azimuthal position of the individual probes at the cylinder bore. Although the probes are uniformly spaced around the circumference, the spark-gap offset from the cylinder axis results in a skewed ray distribution.

For the spark location indicated by the origin of the polar diagram, one would expect the flame to reach probe #8, the nearest, first, and probe #4, the farthest, last. This is clearly not the case for the data presented in the figure, which raises a question about how to interpret data of this type when the ionization probes are not equidistant from the spark gap, and when there are no additional measurements along each radial path between the spark and cylinder wall.

This problem of different path lengths from spark gap to ionization probe is compounded when comparisons are made among data for different operating conditions. The data in Fig. 1 show different behavior between light and heavy load operation, but there is no obvious way to determine which flame arrival times are earlier than "nominal" behavior, and which are later. Normalization by path length to determine an average flame speed (path length divided by flame travel interval) is a simple solution, but one that does not take into account load-related differences in gas temperature, composition, and turbulence intensity, all of which play a significant role in the flame speed. The data in Fig. 1 do

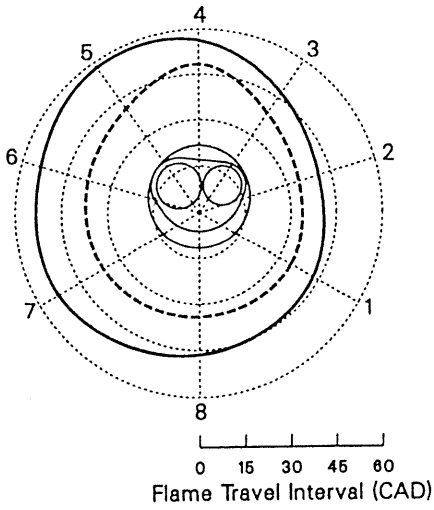

Fig. 1 Ensemble-averaged ionization probe measurements from a production V-6 engine. The flame travel interval is defined as the time from ignition until arrival at the eight probe locations. Solid line: 1300 rpm, light load; dashed line: 2000 rpm, heavy load (from Ref. 6).

show the expected shorter flame travel intervals for heavy load operation, and also shorter intervals toward the side of the combustion chamber with the hotter (and smaller) exhaust valve. However, it is not apparent why the general shapes of the polar plots for light and heavy load are so different.

The inadequacy of assuming a constant flame speed to account for path length differences is illustrated in Fig. 2 for the case of sidewall ignition in a disc-shaped combustion chamber. To obtain these data an ionization probe was placed at different positions along the diameter intersecting the spark gap, yielding the ensemble-averaged flame arrival time at each location, which was then differentiated to generate the solid curve for flame speed. The dashed curve was calculated from the measured cylinder pressure using the two-zone thermodynamic engine model of Borgnakke et al. (8). The agreement between the two is quite good, and the flame speed is seen to vary by more than a factor of two during the combustion event. The focus of this paper is the development of an analytic procedure and graphical presentation format for analyzing flame arrival time measurements that take into account this variation in flame speed.

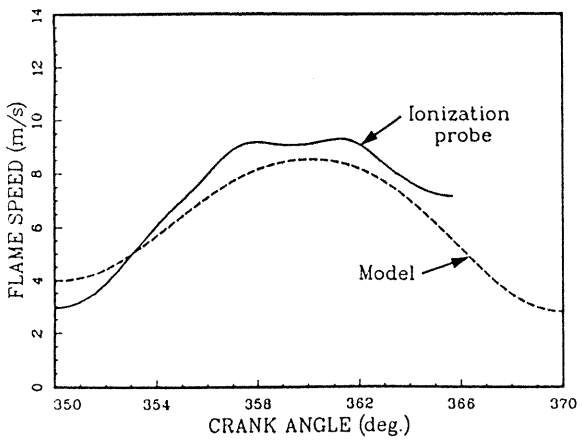

Fig. 2 Flame speed measurements and calculations for sidewall ignition in a disc-shaped combustion chamber (from Ref. 7).

SPHERICAL FLAME MODEL

Phenomenological engine models, such as reviewed by Blumberg et al. (9), are widely used to analyze engine combustion performance. These models attempt to describe complex engine behavior by combining thermodynamic analysis with a collection of physically-based submodels of important processes (e.g., heat transfer, burn rate, and emissions). Typically, combustion is modeled by assuming that the flame is a spherical surface separating the unburned and burned gas regions into two distinct zones of uniform temperature and composition. Because this sphere is described by a radius that grows with time, the model is sometimes termed "quasi-dimensional." However, because of the absence of explicit attention to the fluid mechanics of the combustion process, the model is still basically limited to thermodynamic considerations and is commonly referred to as "thermodynamic" or "zero-dimensional," with time being the only independent variable.

It is the very simplicity of a spherical flame model that has led to its selection herein as the basis of an interpretative tool for flame propagation studies. While real confined flames do not propagate as spherical surfaces, even under initially quiescent conditions, it is mentally easier to look for causes for deviations from sphericity than to try to understand turbulent three-dimensional fluid motions. For combustion in ideal homogeneous mixtures, any nonspherical flame surface can be attributed to one of three forms of fluid motion:

1) Too often unappreciated, it has been realized for many years that premixed gas combustion is accompanied by strong fluid motions. In 1928, Ellis reported the results of several experiments on flame movement in gaseous explosive mixtures. Shown in Fig. 3a is one of his multiple-exposure photographs of flame propagation from two ignition points within a closed tube (10). The mixture was ignited simultaneously at one-quarter and one-half the tube length. Two very important features of confined combustion are illustrated in this figure. First, regarding the expanding flame on the left, it is evident that as the flame approaches the wall the shape becomes nonspherical. This is because the flame propagation speed is greater along the axis of the tube; normal to the tube wall, the expansion velocity must go to zero at the wall. This results in an elongated flame with a surface-to-volume ratio far greater than that of a sphere. Second, regarding the flame on the right, it is seen that the fluid mechanics interaction between the two flames has a significant effect on the location of the flame centroid. In this case the tendency is for the right-side flame to move toward a centered position in the right half of the tube. Shown in Fig. 3b is a two-dimensional simulation (11) of the Ellis experiment, showing how the inclusion of fluid mechanics can lead to a similar behavior, whereas the spherical flame simulation shown in Fig. 3c clearly underestimates the area of the flames.

3a) Multiple exposure photograph by Ellis[1]

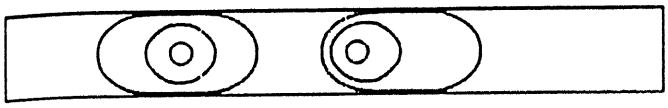

3b) Two-dimensional simulation

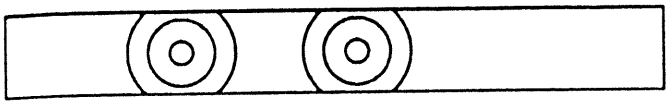

3c) Spherical simulation

Fig. 3 Laminar flame propagation in a closed tube for simultaneous point ignition at one-quarter and one-half the tube length (from Ref. 11).

2) Turbulence is known to wrinkle the flame surface, resulting in an increase in surface area, and thus burning rate, that is critical to the performance of reciprocating engines. However, again often overlooked, the effect of turbulence is not just limited to the smaller scales that wrinkle the flame surface. Large-scale structures on the order of the maximum dimension of the burned volume also can play a significant role, because they can stretch and distort the shape of the burned gas volume; since the surface-to-volume ratio of a sphere is the minimum possible, large-scale distortions of a spherical flame result in an increase in flame area. For such a mechanism to occur, it is necessary that the characteristic velocity of the large-scale structures be on the order of or greater than the burning velocity.

3) Large-scale mean fluid motions such as tumble and swirl can significantly influence flame shape and location. By comparing the evolution of the ideal spherical flame with actual observed behavior, it is often possible to discern bulk fluid motions.

The approach pursued in this paper is to use the measured cylinder pressure to calculate the volume fraction burned as a function of crank angle. For a given combustion chamber geometry and spark location, the radius of the equivalent spherical burned gas volume can then be determined. In practice, the most difficult task to perform is the calculation of the burned gas volume. The mass fraction burned is relatively easy to approximate using the procedure proposed by Rassweiler and Withrow (12) and discussed by Heywood (13), whereby a polytropic compression process is assumed; execution of the procedure is limited mainly by the selection of an appropriate value for the polytropic exponent. To turn the mass fraction burned into a volume fraction is more difficult, since temperatures must be known. This, in essence, requires an accurate estimate of the trapped mass in the cylinder, which cannot be readily measured.

[1]Reproduced from O. C. de C. Ellis, *Fuel in Science and Practice*, Vol. 7, p. 526; 1928, Butterworth & Co. (Publishers) Ltd. ©

Because the focus of this paper is a new procedure for interpreting flame arrival time measurements, and not a new engine combustion model, details of the thermodynamic analysis used are not critical and thus will not be presented. In brief, a modified version of the engine simulation model of Borgnakke et al. (8) was used to analyze the measured cylinder pressure using real gas properties. The heat transfer features of the model were not implemented, and crevice volumes and blowby were also neglected. While it is recognized that these loss mechanisms are important for accurate combustion analysis, they are beyond the scope of this study.

DISCRETIZED SPHERICAL FLAME

Although the disk-shaped combustion chamber used for this study is easily defined analytically, a generalized procedure was developed that could be used to determine the radius of a spherical flame in a volume of arbitrary shape. The procedure is to discretize the combustion volume into finite volume elements, and then for each spark location build a two-dimensional table of spherical flame volume $v(i,j)$ as a function of flame radius $r_f(i)$ and piston displacement $h(j)$, where the indices i and j are explicitly assigned to these two variables, and $h(0)$ is defined to be top center. The discretization process can be done analytically for simple geometries, or with a grid-generating routine available with graphics and finite-element software packages. Once the combustion volume has been discretized, the procedure is to determine the distance from each volume element $\delta v=\delta x\delta y\delta z$ located at (x,y,z) to the spark at (x_s,y_s,z_s), which is the minimum radius of a spherical flame that contains this element. That is,

$$r_f=\sqrt{(x-x_s)^2+(y-y_s)^2+(z-z_s)^2}$$

and $i=r_f/\delta r_f$, where δr_f is the discretized incremental size of the flame-radius array. Thus,

$$v(i,0)=\sum \delta v \text{ for all } r_f \le r_f(i)$$

This procedure needs to be repeated for all $h(j)$, but this is a trivial analytic task once the clearance volume portion of the table has been created, since it is necessary to simply append the burned volume in the sweep volume.

Presented in Fig. 4 are look-up table calculations for a disk-shaped combustion chamber with the spark at the top surface at the radial position $r/r_b=0.6$, where r_b is the bore radius. The piston location variable $h(j)$ was discretized in 100 uniform increments over the sweep distance, and for each piston location the flame radius $r_f(i)$ was discretized in 100 uniform increments over the maximum possible flame radius. It took slightly less than two minutes for a 486/33 microprocessor with math coprocessor to calculate the table. This considerably lengthy computation period emphasizes the advantages of a look-up table approach to this problem.

To apply the procedure, the measured cylinder pressure is input to the two-zone combustion model to obtain the burned gas volume as a function of crank angle, which is

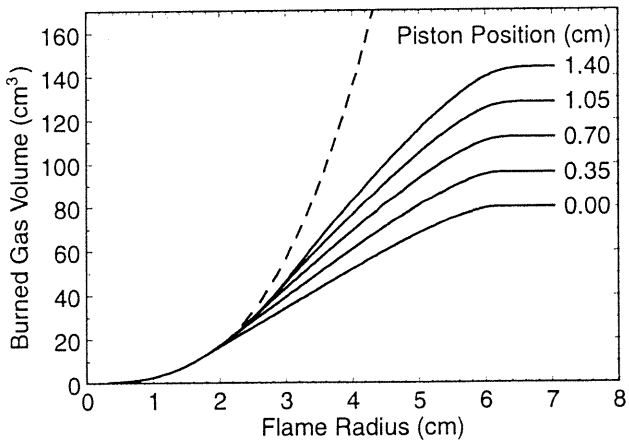

Fig. 4 Graphic presentation of the lookup table for burned gas volume as a function of flame radius and piston position (defined as distance from top center). The dashed curve indicates the volume of a hemisphere uninterrupted by the confines of the combustion chamber.

then used with linear interpolation of the look-up table to obtain the flame radius. The measured pressure record and combustion model results for the mass and volume fraction burned are given in Fig. 5 for the engine conditions to be described next.

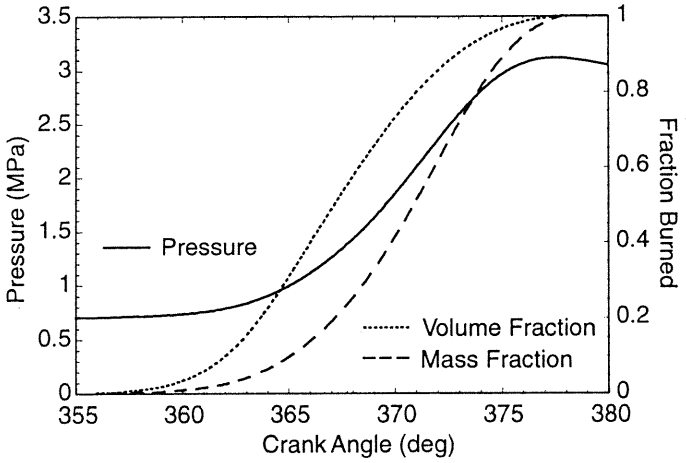

Fig. 5 Measured cylinder pressure and calculated results for mass and volume fraction burned. Ignition was at 5 degrees before top center.

EXPERIMENTAL DESCRIPTION

The measurements were made in the Sandia side-valved research engine shown schematically in Fig. 6. The engine was run at 600 rpm on propane fuel at stoichiometric conditions. The engine was fueled every cycle, but ignited only every third cycle, which results in a mixture that is essentially free of burned gas products. Because of the clearance necessary to accommodate the valves in the side wall of the combustion chamber, the compression ratio is only 5.4

The ionization probes were integral with the head gasket, which was a fiber-reinforced polyimide printed-circuit-board (6). The analog signals from the eight ionization

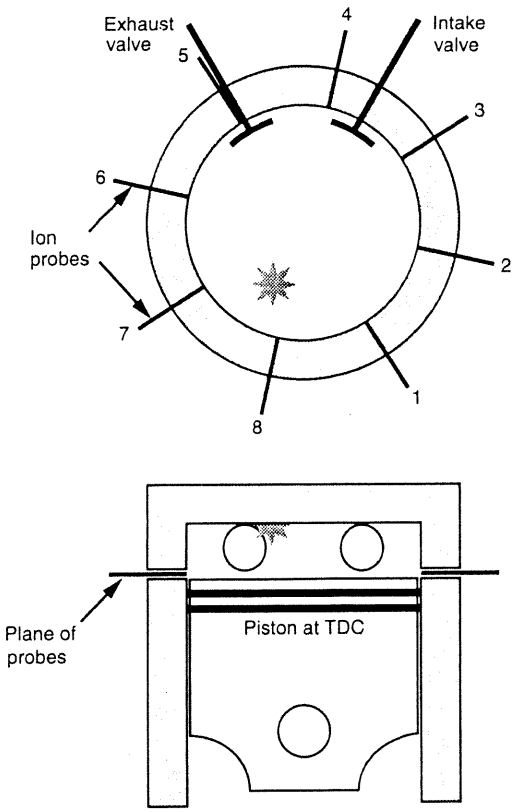

Fig. 6 Schematic of side-valved research engine, showing the spark and ionization-probe locations.

probes and a pressure transducer were simultaneous recorded by a personal computer for 100 engine cycles. The flame arrival times were then determined by interrogation of the amplitude of the ionization probe signals, and ensemble averages were computed for these measurements and the cylinder pressure history.

RESULTS

Flame arrival time measurements for ignition at the two-thirds radial position are shown in Fig. 7. A spline-fit interpolation procedure has been used to generate the smooth curve connecting the eight discrete measurements. Note that a distorted polar diagram is used to show the true direction from the offset spark gap to the probes located at the cylinder wall (indicted by the bold circle). These data show the expected result of earliest arrival of the flame at the probes closest to ignition (#'s 6 and 7), and late arrival at the most distant probes (#'s 3 and 4). However, it is clearly apparent that flame arrival is unexpectedly late at probe #2.

These eight flame arrival time measurements are presented again in the left side of Fig. 8 as the square symbols, indicating the radial distance from the spark to each probe as a function of the time of actual flame arrival. The solid curve is the spherical flame radius obtained from the measured pressure via thermodynamic analysis and the lookup table. For all measurements lying to the left of this curve, the spherical flame is calculated to reach the probe *after* measured flame arrival; for all measurements to the right, spherical flame arrival is *earlier* than measured. Thus, the flame-

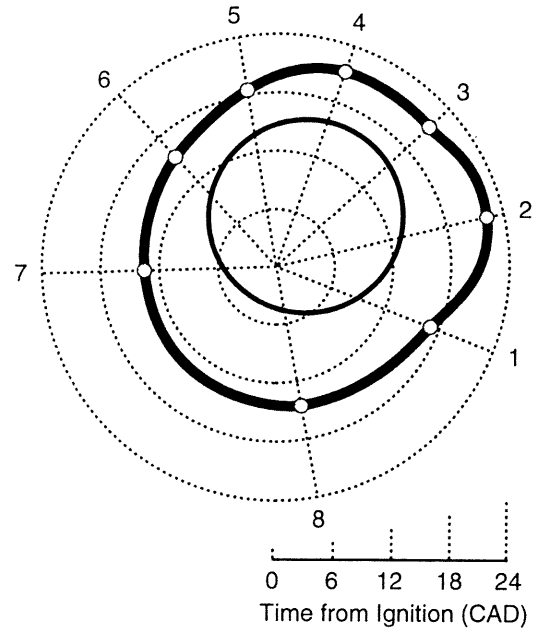

Fig. 7 Ensemble-averaged flame arrival time measurements obtained from ionization probes installed in the head gasket.

radius curve serves as a reference condition for interpretation of the actual data. These results show that the spherical flame model corresponds well with the measured flame arrival times for probes #3-6, but that the actual flame reached probes #1, 2, 7 and 8 much later than predicted by the spherical flame.

The diagrams in the right side of Fig. 8 graphically illustrate the shape and location of the ideal spherical flame at the instant each probe detected the actual flame. In the top views, the shaded region indicates the intersection of the burned volume with the plane of the ionization probes; the second, singular curved line indicates the flame radius in the spark plane. The spark location is indicated by the star-like symbol, and the straight line marks the path to the probe detecting the flame at that instant. For each diagram, solid circles are used for all ionization probes engulfed in flame, and open circles indicate probes still in the unburned gas.

The side views in Fig. 8 are, unfortunately, somewhat more complicated. Because the intent is to show the spherical flame front shape in the vicinity of each probe at the time of actual flame arrival, these views are a cross-section defined by the path between the spark and each ionization probe. For uniformity, the active ionization probe is always shown on the right-hand side of the figure, indicated by the short horizontal line, and the **E** or **L** directly above it corresponds to either early or late arrival of the spherical flame relative to the measurement. The upper number in the side views is the ratio of the spherical flame radius to the radial distance from the spark to the ionization probe (such that values less than unity correspond to late arrival of the spherical flame relative to measured arrival), and the lower number is the crank angle of measured flame arrival relative to ignition.

The late arrival of the actual flame at probe locations 7 and 8, relative to the ideal spherical flame, is the direct result of the strong influence that walls and fluid motion have on the shape and location of the burned gas volume. As shown earlier in Fig. 3, the true tendency of a confined flame is to move away from walls into open space. This phenomenon is more prevalent early in the combustion process, when the volume fraction burned is still small; as combustion nears completion, this phenomenon becomes negligible.

A second feature of the combustion process revealed by this figure is the existence of counter-clockwise swirl motion. This is indicated by the earlier arrival of the flame at locations 7 relative to 8, and 6 relative to 1. This behavior be-

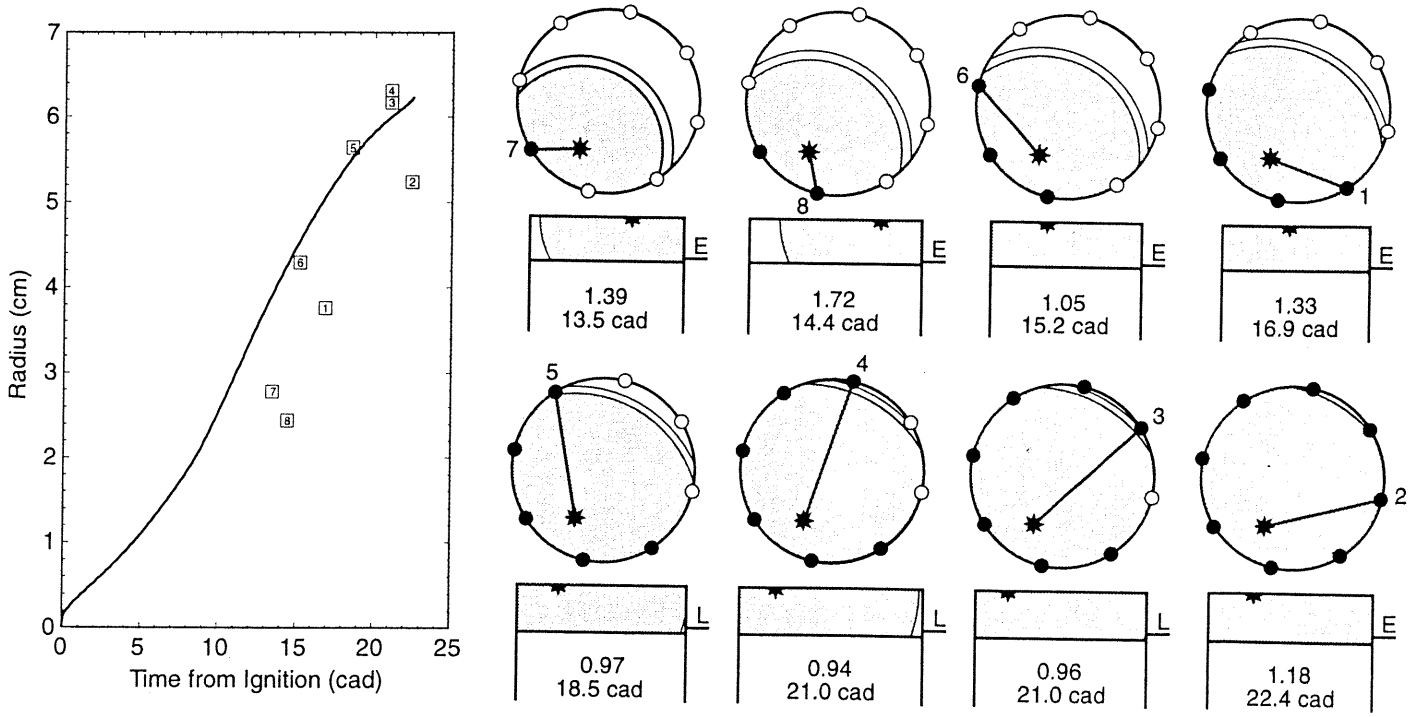

Fig. 8 Comparison of the ideal spherical flame with ionization probe measurements for offset ignition.

comes even more evident near the end of combustion, as indicated by the sequential arrival of the flame at locations 5 through 2. This swirl motion is also responsible for detection of the flame by probe #'s 6 and 5 at times very close to the spherical flame, whereas probe #'s 1 and 2 detect the flame very late; for the former, swirl is counteracting the wall-repulsion phenomenon, whereas it is enhancing it at the latter two locations.

CONCLUSIONS

Although the results presented clearly reveal the fallacy of the spherical flame assumption, a graphic presentation of the differences between the ideal spherical flame and ionization probe measurements of actual flame arrival is a useful technique for data interpretation. The alternative of a fully three-dimensional simulation with coupled fluid mechanics would be extremely costly and limited by the ability of the model to correctly simulate a complex fluid flow. By using a spherical flame model, at least one knows exactly what the limitations of the model are. Implementation of a spherical model by the lookup table procedure described is also straightforward and computationally fast, and readily amenable to computerized design techniques.

It is important to keep in mind that for this work the spherical flame radius was determined from the measured pressure. Thus, even though the spherical flame assumption showed extremely poor agreement with measurements by ionization probes close to an offset spark plug, later in the combustion event agreement can still be good. This will not be the case when a spherical flame model is used in a predictive mode. Instead, the spherical model will predict early truncation of the flame surface by the walls, resulting in a burning rate that is much too slow. This problem is typically compensated for by an exaggerated turbulence enhancement of the flame speed, which is one of the root causes of the great disparity in turbulent flame propagation models.

ACKNOWLEDGMENT

The author is indebted to Prof. Claus Borgnakke, University of Michigan, Ann Arbor, for providing the two-zone engine simulation model used for this study. The particular version of the model used was developed during a sabbatical visit to Sandia in 1985. Also to be thanked is Gary Hubbard for his guidance in formulating the flame radius table-look-up procedure, and Paul Miles and Pamela Barr for many helpful discussions. This work was performed at the Combustion Research Facility of the Sandia National Laboratories, and was funded by the U.S. Department of Energy, Office of Transportation Technologies.

REFERENCES

1. Schnauffer, K., "Engine-Cylinder Flame-Propagation Studied by New Method", *SAE J. (Trans.)*, Vol. 34, p. 17, 1934.
2. Curry, S., "A Three-Dimensional Study of Flame Propagation in a Spark Ignition Engine," *Trans. SAE*, Vol. 71, p. 628, 1963.
3. Spicher, U. and Velji, A., "Measurements of Spatial Flame Propagation and Flow Velocities in a Spark Ignition Engine," *Twentieth Symposium (International) on Combustion*, The Combustion Institute, p. 19, 1984.
4. Spicher, U. and Krebs, R., "Optical Fiber Technique as a Tool to Improve Combustion Efficiency," *Trans. SAE*, Vol. 99, Sec. 3, p. 2236, 1990.
5. Witze, P. O., "Cycle-Resolved Multipoint Ionization Probe Measurements in a Spark Ignition Engine," *Trans. SAE*, Vol. 98, Sec. 3, p. 2074, 1989.
6. Nicholson, D. E. and Witze, P. O., "Flame Location Measurements in a Production Engine Using Ionization Probes Embodied in a Printed-Circuit-Board Head Gasket," SAE Paper No. 930390, 1993.
7. Witze, P. O. and Mendes-Lopes, J. M. C., "Direct Measurement of the Turbulent Burning Velocity in a Homogeneous-Charge Engine," *Trans. SAE*, Vol. 95, Sec. 6, p. 540, 1986.
8. Borgnakke, C., Davis, G. C. and Tabaczynski, R. J., "Predictions of In-Cylinder Swirl Velocity and Turbulence Intensity for an Open Chamber Cup in Piston Engine," *Trans. SAE*, Vol. 90, p. 964, 1981.
9. Blumberg, P. N., Lavoie, G. A. and Tabaczynski, R. J., "Phenomenological Models for Reciprocating Internal Combustion Engines," *Prog. Energy Combust. Sci.*, Vol. 5, p. 123, 1979.
10. Ellis, O. C. de C., "Flame Movement in Gaseous Explosive Mixtures (Part 9)," *Fuel in Science and Practice*, Vol. 7, p. 526, 1928.
11. Barr, P. K. and Witze, P. O., "Some Limitations to the Spherical Flame Assumption Used in Phenomenological Engine Models," SAE Paper No. 880129, 1988.
12. Rassweiler, G. M. and Withrow, L., "Motion Pictures of Engine Flames Correlated with Pressure Cards," *Trans. SAE*, Vol. 42, p. 185, 1938.
13. Heywood, J. B., Internal Combustion Engine Fundamentals, McGraw Hill, New York, 1988, p. 385.